

Galactic Orbits of Interstellar Objects

Shokhruz Kakharov and Abraham Loeb

Astronomy Department, Harvard University, 60 Garden St., Cambridge, MA 02138, USA,
e-mail: shokhruzbekkakharov@college.harvard.edu; aloeb@cfa.harvard.edu

ABSTRACT

Context. The first interstellar objects, such as ‘Oumuamua, Borisov and IM1, were discovered over the past decade.

Aims. We follow the trajectories of known interstellar objects in the gravitational potential of the Milky Way galaxy to constrain their possible origin.

Methods. We initiate the trajectories based on the measured velocities of the interstellar objects relative to the Local Standard of Rest. Since the scale-height of stars in the Milky-Way disk increases with age, we use the vertical excursion of each interstellar object from the Milky-Way disk mid-plane to constrain their likely age.

Results. The small vertical extent of ‘Oumuamua’s past trajectory suggests that it originated near the mid-plane of the thin disk, implying a likely age younger than 1–2 Gyr. The maximal excursion of the comet Borisov is similar to that of the Sun, suggesting a similar age. The meteor IM1 exhibits yet larger vertical excursions, suggesting an older source. Finally, we show that human-made interstellar probes, like Voyager 1 or Pioneer 10 will arrive at the opposite side of the Milky Way disk relative to the Sun in ~ 2 Gyr and return to the vicinity of the Sun before it becomes a red giant.

Key words. interstellar objects – galactic trajectories – origins

1. Introduction

The discovery of interstellar objects like ‘Oumuamua and Borisov over the past decade has sparked significant interest in understanding their origins and dynamics (see reviews by Siraj & Loeb (2022a), Jewitt and Seligman (2023), Jewitt (2024), and references therein). A fundamental unknown is the likely source of each of these objects (Bailer-Jones et al. 2018, 2020). Constraining the sources could shed light on the nature of these interstellar objects and the astrophysical processes that created them (see, for example, Zhang & Lin (2020) or Loeb & MacLeod (2024)).

In this paper, we numerically integrate the trajectories of interstellar objects back in time in the gravitational potential of the Milky-Way as a way to relate them to potential stellar populations. For simplicity, we ignore transient gravitational features such as spiral arms and the Galactic bar. This is a reasonable approximation for orbits in the outer part of the Galactic disk.

By integrating the orbits of these objects back in time, we are able to constrain the spatial region of their potential sources within the Milky Way. These constraints limit the possible birthplaces of the different interstellar objects and provide insights into the Galactic environment from which they originated.

Since the scale-height of stars in the Milky-Way disk increases with age, we use the vertical excursion of each interstellar object from the Milky-Way disk mid-plane to constrain its likely age. Any dynamical pumping of the stellar scale-height by gravitational perturbations from satellite galaxies or star clusters, would affect interstellar objects and stars alike since both populations are collisionless. Hence, our constraints apply to the full age of the interstellar objects irrespective of their travel time.

We also apply the same numerical approach to calculating the future trajectories of the interstellar probes launched by NASA decades ago, Voyager 1 & 2 and Pioneer 10 & 11.

The organization of this paper is as follows. Section 2 describes our method of calculation and the resulting Galactic trajectories for the individual interstellar objects, with subsections dedicated to Borisov (§2.2), ‘Oumuamua (§2.3) and IM1 (§2.4). In Section 3, we use the resulting vertical excursion of these trajectories to derive the probability distribution for the likely age for each of these objects. Section 5 considers the future trajectories of human-made interstellar probes. Finally, we summarize the implications of our results in Section 6.

2. Galactic Trajectories of Interstellar Objects

2.1. Method of Calculation

Our numerical integration is based on the OrbitIntegrator from GalPot, which utilizes the MWPotential2014 model from McMillan (2017) to simulate the gravitational potential of the Milky Way galaxy. We assume a circular velocity of 233 km s^{-1} and an orbital radius of 8.3 kpc for the Local Standard of Rest (LSR) around the Galactic center, consistently with the latest Gaia data (Pöder et al. 2023). We initiate the trajectories from the velocity of each interstellar object relative to the LSR and follow them back in time for 10 Gyr, roughly the age of the Milky Way disk (Fantin et al. 2019). The code uses the NumPy’s `linspace` function that defines the relevant timescale, and then integrates the orbits using the OrbitIntegrator’s `getOrbitPath` and `Stats` method. The resulting orbit paths are extracted and plotted using Matplotlib, with separate plots showing the radial distance R , vertical excursion from the disk mid-plane z , and azimuthal angle ϕ , as functions of time. The code also calculates the evolution of the velocity components v_R , v_z , and v_ϕ as functions of time.

In order to convert the velocity measurements in the Solar system to the Galactic frame of reference, we incorporate the motion of the Sun relative to the Local Standard of Rest

(LSR), with the Galactic components: $U_{\odot} = 10.79 \pm 0.56 \text{ km s}^{-1}$, $V_{\odot} = 11.06 \pm 0.94 \text{ km s}^{-1}$, and $W_{\odot} = 7.66 \pm 0.43 \text{ km s}^{-1}$ (Robin et al. 2022). Before entering the solar system, Borisov's velocity was $(U, V, W) = (33.1, -6.8, 8.3) \text{ km s}^{-1}$, while 'Oumuamua's velocity relative to the Sun is $(U - U_{\odot}, V - V_{\odot}, W - W_{\odot}) = (-11.457 \pm 0.009, -22.395 \pm 0.009, -7.74 \pm 0.011) \text{ km s}^{-1}$ (Bailer-Jones et al. 2020; Mamajek 2017). For the interstellar meteor, IM1, we adopt $(U, V, W) = (32.7 \pm 5.8, -4.5 \pm 1.5, 26.1 \pm 2.0) \text{ km s}^{-1}$ (Siraj & Loeb 2022b).

2.2. Comet Borisov

The past evolution of the distance of the interstellar comet Borisov from the Sun is shown in figure 1. The Sun-Borisov separation follows a period of about 3.2 Gyr, with Borisov being on the other side of the Milky-Way disk relative to the Sun about 1.6 Gyr ago.

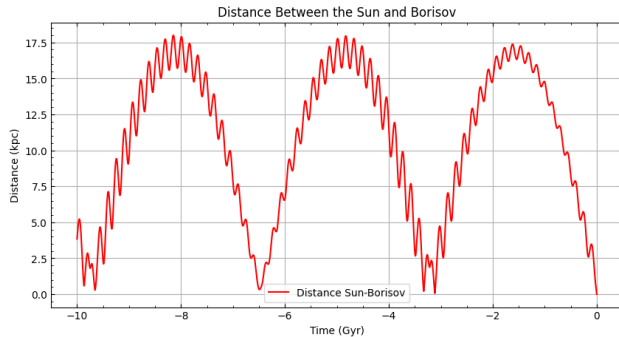


Fig. 1. Distance of the comet Borisov from the Sun back in time with the present time represented by 0.

The radial (R) and vertical (z) extent of Borisov's trajectory relative to the Galactic plane over the past 10 Gyr are depicted in figure 2 (orange) and resemble the corresponding ranges for the Sun (blue).

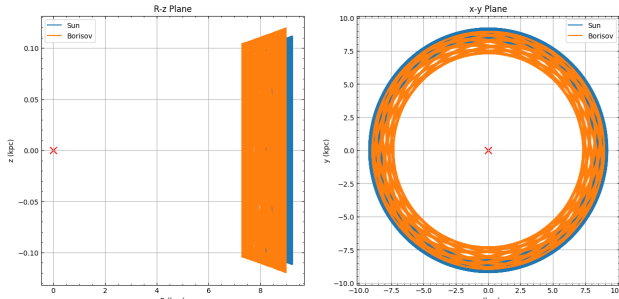


Fig. 2. Trajectory of the comet Borisov in the $R - z$ and $x - y$ plane of the Milky-Way disk.

2.3. 'Oumuamua

The past evolution of the distance of the interstellar object 'Oumuamua from the Sun is shown in figure 3. The 'Oumuamua-Sun separation follows a period of about 2.2 Gyr, with 'Oumuamua being on the other side of the Milky Way disk relative to the Sun about 1.1 Gyr ago.

The radial (R) and vertical (z) extent of 'Oumuamua's trajectory relative to the Galactic plane over the past 10 Gyr are depicted in figure 4 (orange). As a result of its low vertical ve-

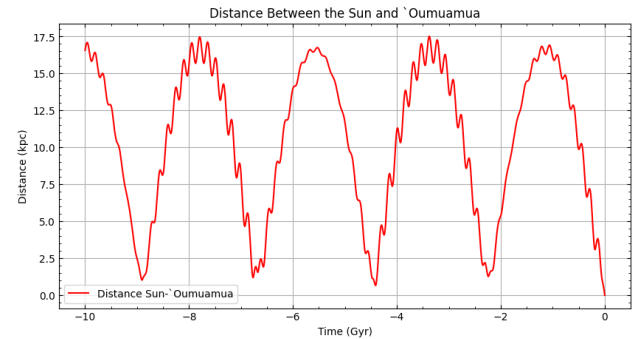


Fig. 3. Distance of 'Oumuamua from the Sun back in time.

locity relative to the LSR, the vertical excursion of 'Oumuamua is a factor of ~ 6 smaller than that of the Sun (blue).

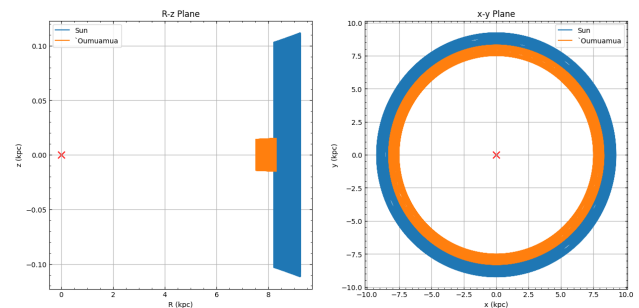


Fig. 4. Trajectory of 'Oumuamua in the $R - z$ and the $x - y$ plane of the Milky-Way disk.

2.4. IM1

The past evolution of the distance of the interstellar meteor IM1 from the Sun is shown in figure 5. The IM1-Sun separation follows a period of about 4.3 Gyr, with IM1 being on the other side of the Milky Way disk relative to the Sun about 2.15 Gyr ago.

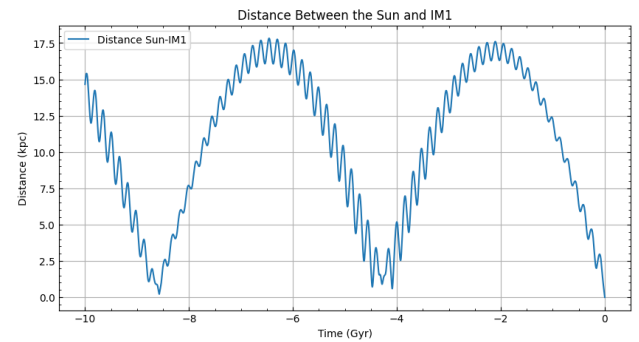


Fig. 5. Distance of IM1 from the Sun back in time.

The radial (R) and vertical (z) extent of IM1's trajectory relative to the Galactic plane over the past 10 Gyr are depicted in figure 6 (orange). As a result of its high vertical velocity, the vertical excursion of IM1 is ~ 2.5 times larger than that of the Sun (blue).

3. Probability Distribution of Age

Next, we evaluate the probability distribution $p(t)$ (with a unit normalization $\int p(t)dt = 1$) for the age t of the interstellar ob-

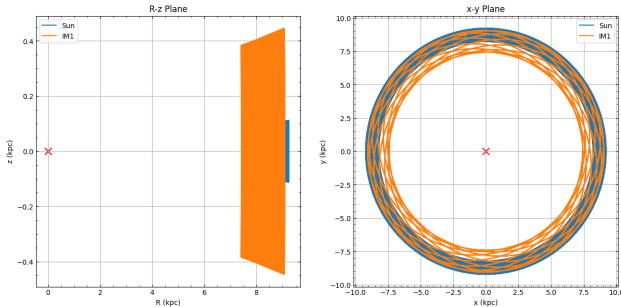


Fig. 6. Trajectory of IM1 in the $R - z$ and the Galactic $x - y$ plane.

jects, assuming that they originated from stars. We base our analysis on the extent of their vertical excursions, quantified by the maximum vertical (z) value that their orbits span, z_{\max} , given that the scale-height of stars depends on their age.

3.1. Star Formation Rate (SFR) as a Function of Lookback Time

We start from the empirically-calibrated star formation rate (SFR) history of the Milky-Way disk, based on the age distribution of white dwarfs (Fantin et al. 2019). The SFR is divided into two parts: a flat component from lookback time of 0 to 9 Gyr, plus a Gaussian component centered on 10 Gyr. For the flat component, we adopt a constant value of SFR_{linear} , whereas the Gaussian part is described by,

$$SFR_{\text{Gaussian}}(t) = SFR_{\text{peak}} \times \exp\left(-\frac{1}{2}\left(\frac{t - t_{\text{peak}}}{\sigma}\right)^2\right), \quad (1)$$

where $SFR_{\text{peak}} = 3SFR_{\text{linear}}$, $t_{\text{peak}} = 10$ Gyr, and $\sigma = 0.5$ Gyr. Figure 7 shows the resulting age distribution of stars, plotted in 1 Gyr bins

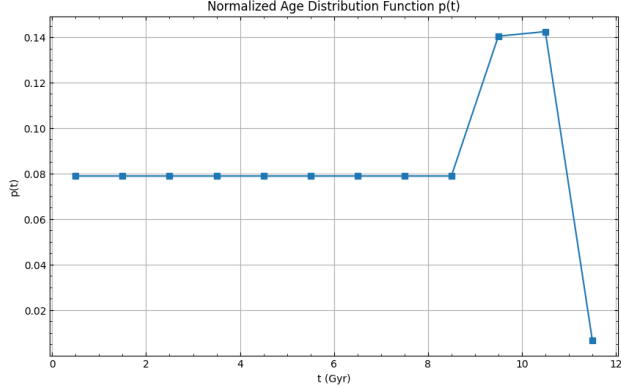


Fig. 7. Probability distribution of age, $p(t)$ in units of Gyr^{-1} , for the stars in the Milky Way disk, based on figure 9 in Fantin et al. (2019).

The stellar mass formed in each temporal bin of width $\Delta t = 1$ Gyr, is given by

$$\Delta M(t) = SFR_{\text{binned}}(t) \times \Delta t. \quad (2)$$

The current number density of disk stars at the Galactic orbital radius of the Sun follow an exponential vertical distribution relative to the mid-plane, $\propto \exp\{-|z/h|\}$, with a scale-height, $h(t)$, that depends on their age t . We adopt the observed $h(t)$ from Cukanovaite et al. (2023) and combine it with the star formation

history described above to calibrate the fraction of stars with any given age.

To quantify the age distribution of stars within the vertical excursion of each interstellar object, we determine the number of stars residing in each age bin up to the maximum z value sampled by the object's trajectory, denoted by z_{\max} ,

$$\Delta N(t) \propto \Delta M(t) \left(1 - \exp\left(-\frac{z_{\max}}{h(t)}\right)\right), \quad (3)$$

where z_{\max} is the maximum vertical height for the object.

To obtain a unit normalization of our probability distribution of ages, we find the total number of stars within the given z range as,

$$N_{\text{total}} = \sum_i \Delta N(t_i), \quad (4)$$

where N_{total} represents the total number of stars and $\Delta N(t)$ denotes the number of stars in the age bin centered at age t . The summation is performed over all age bins t_i given the constraint of z_{\max} .

The normalized age distribution function $p(t)$ is then calculated from the relation,

$$p(t_i) = \frac{\Delta N(t_i)}{N_{\text{total}} \Delta t}. \quad (5)$$

3.2. Likelihood of Ages for individual Interstellar Objects

Figure 8 shows the probability distribution of likely ages for the comet Borisov, which straddles the age of the Sun at 4.6 Gyr.

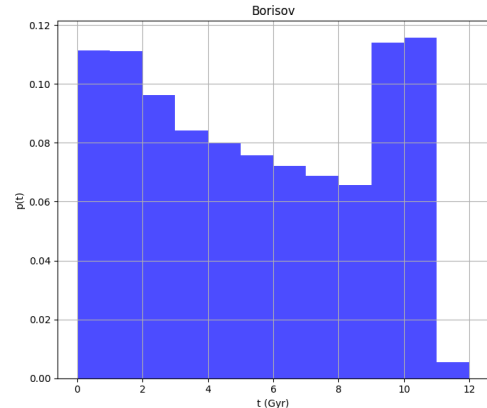


Fig. 8. Probability distribution of age, $p(t)$ in units of Gyr^{-1} , for the interstellar comet Borisov with $z_{\max} = 0.12$ kpc.

In contrast, ‘Oumuamua is much younger with a likely age of 1-2 Gyr, based on its much smaller value of z_{\max} , as shown in Figure 9.

Finally, IM1 follows the probability distribution of the entire Galactic disk population, $SFR(t)$, because of its large value of z_{\max} , as shown in Figure 10.

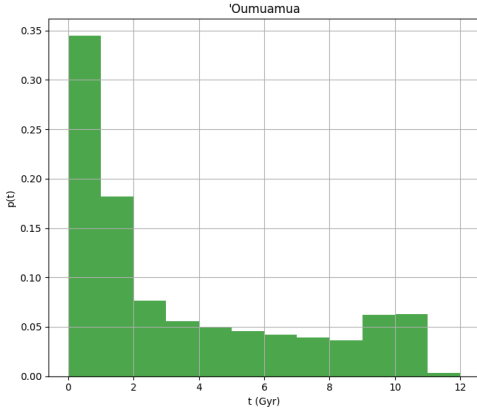


Fig. 9. Probability distribution of age, $p(t)$ in units of Gyr^{-1} , for Oumuamua with $z_{\text{max}} = 0.015 \text{ kpc}$.

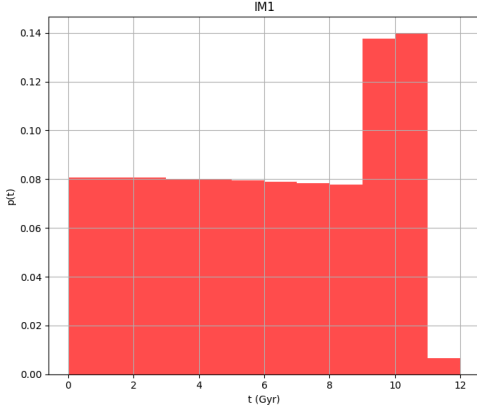


Fig. 10. Probability distribution of age, $p(t)$ in units of Gyr^{-1} , for IM1 with $z_{\text{max}} = 0.45 \text{ kpc}$.

4. Interstellar Probes

Finally, we derive the future trajectories of the first four interstellar probes, Voyager 1 & 2, Pioneer 10 & 11, which are making their way out of the Solar system. For each probe, we adopt the current velocity relative to the Sun based on the following directions of motion (right ascension and declination) and speeds (Bailer-Jones & Farnocchia 2019):

- Voyager 1: $\alpha = 262.8760^\circ$, $\delta = 12.3199^\circ$, $v = 16.6048 \text{ km s}^{-1}$.
- Voyager 2: $\alpha = 316.2717^\circ$, $\delta = -67.5491^\circ$, $v = 14.8550 \text{ km s}^{-1}$.
- Pioneer 10: $\alpha = 83.4169^\circ$, $\delta = 26.2171^\circ$, $v = 11.3149 \text{ km s}^{-1}$.
- Pioneer 11: $\alpha = 291.8277^\circ$, $\delta = -9.2212^\circ$, $v = 10.4439 \text{ km s}^{-1}$.

We transformed the velocity vectors to Cartesian Galactic coordinates and added the velocity vector of the Sun. Below we describe the resulting trajectory for each of the probes.

4.1. Voyager 1

The future evolution of the distance of the Voyager 1 from the Sun is shown in figure 11. The separation follows a period of about 3.6 Gyr, with Voyager reaching the other side of the Milky Way disk relative to the Sun in about 1.8 Gyr.

The radial (R) and vertical (z) extent of Voyager 1's trajectory relative to the Galactic plane in the next 10 Gyr are depicted in figure 12 (orange) and resemble the corresponding ranges for the Sun (blue).

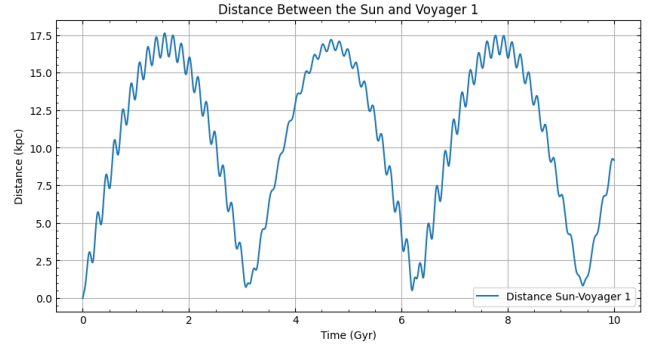


Fig. 11. Distance of Voyager 1 from the Sun as a function of future time, with 0 representing the present time.

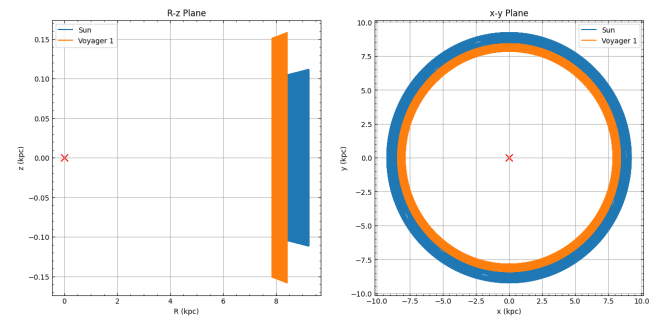


Fig. 12. Trajectories of Voyager 1 in the $R - z$ and the Galactic $x - y$ plane.

4.2. Voyager 2

The future evolution of the distance of the Voyager 2 from the Sun is shown in figure 13. The Voyager 2-Sun separation follows a period of about 13 Gyr, comparable to the age of the Universe, with the probe reaching the other side of the Milky Way disk relative to the Sun in about 6.5 Gyr. Interestingly, Voyager 2 is predicted to arrive within 0.1 kpc from the Sun on its first return.

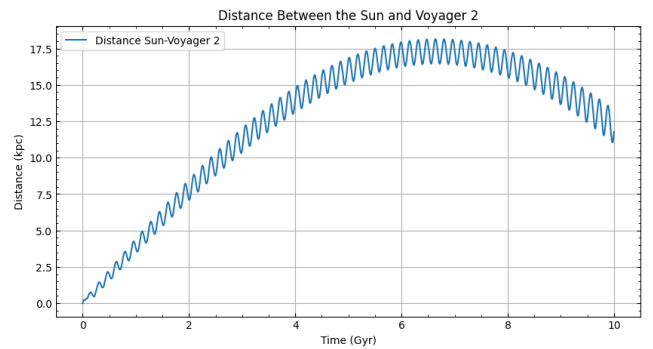


Fig. 13. Distance evolution of Voyager 2 from the Sun.

The radial (R) and vertical (z) extent of Voyager 2's trajectory relative to the Galactic plane in the next 10 Gyr are depicted in figure 14 (orange) and resemble the corresponding ranges for the Sun (blue).

4.3. Pioneer 10

The future evolution of the distance of the Pioneer 10 from the Sun is shown in figure 15. The separation follows a period of about 4.6 Gyr, with Pioneer 10 reaching the other side of the Milky Way disk relative to the Sun in about 2.3 Gyr.

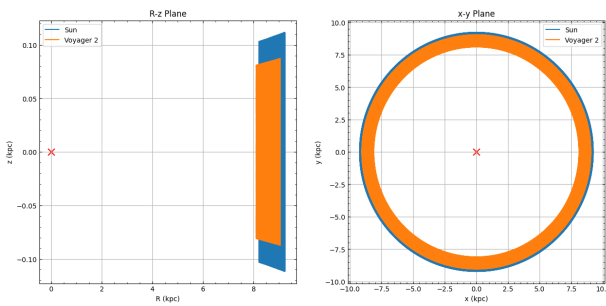


Fig. 14. Trajectories of Voyager 2 in the $R - z$ and the Galactic $x - y$ plane.

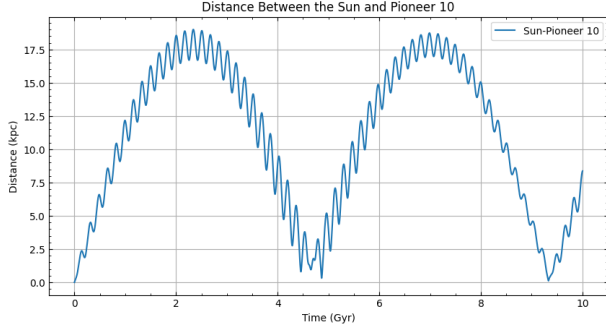


Fig. 15. Distance evolution of Pioneer 10 from the Sun.

The radial (R) and vertical (z) extent of Pioneer 10's trajectory relative to the Galactic plane in the next 10 Gyr are depicted in figure 16 (orange) and resemble the corresponding ranges for the Sun (blue).

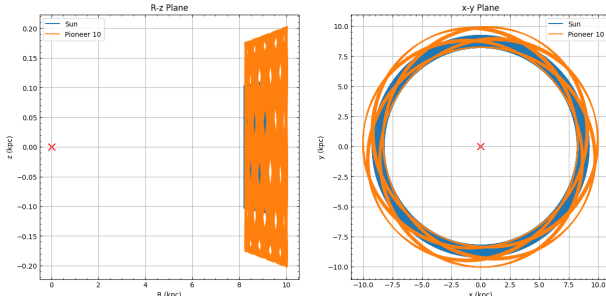


Fig. 16. Trajectories of Pioneer 10 in the $R - z$ and the Galactic $x - y$ plane.

4.4. Pioneer 11

The future evolution of the distance of the Pioneer 10 from the Sun is shown in figure 17. The separation follows a period of about 5 Gyr, with Pioneer 12 reaching the other side of the Milky Way disk relative to the Sun in about 2.5 Gyr.

The radial (R) and vertical (z) extent of Pioneer 10's trajectory relative to the Galactic plane in the next 10 Gyr are depicted in figure 18 (orange) and resemble the corresponding ranges for the Sun (blue).

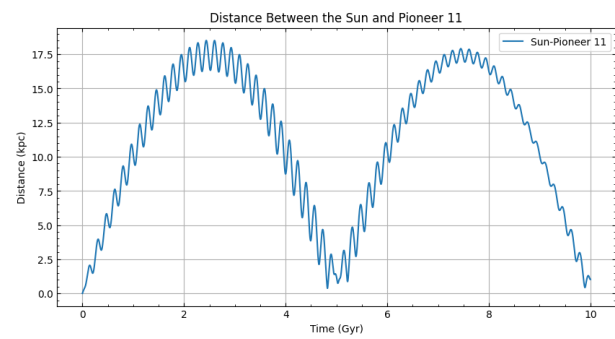


Fig. 17. Distance evolution of Pioneer 11 from the Sun.

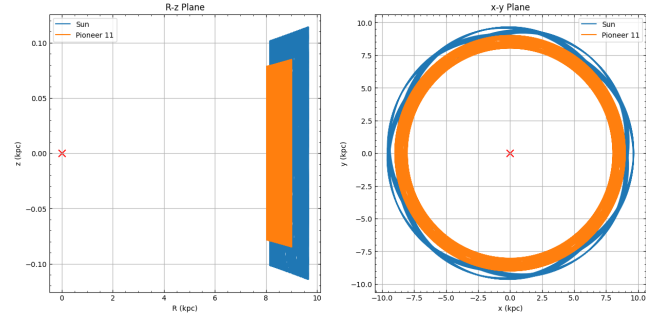


Fig. 18. Trajectories of Pioneer 11 in the $R - z$ and the Galactic $x - y$ plane.

5. Conclusions

We have integrated the Galactic trajectories of known interstellar objects back in time. The vertical extent of the trajectory of 'Oumuamua suggests that it originated near the disk mid-plane of the thin disk, where the ages of most stars are below 1–2 Gyr. In contrast, the comet Borisov's vertical excursion is similar to that of the Sun, suggesting a similar age. Given its highest vertical excursions, the putative source star of IM1 is most likely the oldest.

Over many orbital times, the trajectories are expected to migrate radially as a result of transient features like spiral arms or the Galactic bar (Sellwood & Binney 2002). Our constraints apply to the full age of the interstellar objects, because they respond just like the underlying stellar population to gravitational perturbations that pump up their scale-height over time.

Our constraints on the ages of the various objects represent upper limits because the velocity dispersion of the interstellar objects includes both the velocity dispersion of their parent stars and the dispersion in their characteristic ejection speed away from their birth system.

In addition, our calculations indicate that the interstellar probes Voyager 1 and Pioneer 10 will reach the opposite side of the Milky-Way disk relative to the Sun in ~ 2 Gyr from now, and will return to the Solar vicinity in ~ 4 Gyr. This future return will occur long before the Sun will become a red giant star in ~ 7.6 Gyr (Schröder & Smith 2008).

Acknowledgements. We thank Morgan MacLeod for helpful comments on the manuscript. This work was supported in part by Harvard's Institute for Theory & Computation, the Harvard Astronomy and Physics departments, the BHI and the Galileo Project.

References

- Bailer-Jones C. A. L., Farnocchia D., Meech K. J., Brasser R., Micheli M., Chakrabarti S., Buie M. W., et al., 2018, AJ, 156, 205
- Bailer-Jones, C. A. L., & Farnocchia, D. 2019, RNAAS, 3, 59
- Bailer-Jones, C. A. L., Farnocchia, D., Ye, Q., Meech, K. J., Micheli, M. 2020, ApJ, 903, 5
- Bailer-Jones, C. A. L., Farnocchia, D., Ye, Q., Meech, K. J., Micheli, M. 2020, A&A, 634, A14

Belokurov, V., et al. 2018, MNRAS, 478, 611
 Sellwood J. A., Binney J. J., 2002, MNRAS, 336, 785
 Cukanovaite, E., Tremblay, P.-E., Toonen, S., et al. 2023, MNRAS, 522, 1643
 Deason, A. J., et al. 2013, MNRAS, 434, 3348
 Donlon, T., et al. 2024, MNRAS, 531, 1422
 Fantin, N. J., Côté, P., McConnachie, A. W., et al. 2019, ApJ, 887, 148
 Gaia Collaboration 2018, A&A, 616, A1
 Gondoin, P. 2023, A&A, 678, A39
 Jewitt, D., Seligman, D. Z. 2023, Annual Review of Astronomy and Astrophysics
 61, 197
 Jewitt, D. 2024. Interstellar Objects in the Solar System. arXiv e-prints
 Johnson, A., et al. 2019, ApJ, 874, 100
 Loeb A., MacLeod M., 2024, A&A, 686, A123
 Mazzi, A., et al. 2024, A&A, in press
 Mamajek, E. 2017, Research Notes of the American Astronomical Society, 1, 21
 McMillan, P. J. 2017, MNRAS, 465, 76
 Pöder, S., Benito, M., Pata, J., et al. 2023, A&A, 676, A134
 Robin, A. C., Bienaymé, O., Salomon, J. B., et al. 2022, A&A, 667, A98
 Schröder K.-P., Smith R. C., 2008, MNRAS, 386, 155
 Siegert, T. 2019, A&A, 632, L1
 Siraj A., Loeb A., 2022a, AsBio, 22, 1459
 Siraj A., Loeb A., 2022b, ApJ, 939, 53
 Sousa, S. G., Santos, N. C., Adibekyan, V. Zh., et al. 2024, A&A, in press
 Zhang Y., Lin D. N. C., 2020, NatAs, 4, 852